6

Ionian mountains and tectonics: Insights into what lies beneath Io's lofty peaks

Elizabeth P. Turtle, Windy L. Jaeger, and Paul M. Schenk

6.1 INTRODUCTION

A world of extremes, Io, in addition to displaying extensive volcanism, supports some of the highest mountains in the Solar System. Yet, in an apparent paradox, very few of the mountains actually resemble volcanoes; the majority of the towering peaks appear to be tectonic structures: uplifted and sometimes tilted blocks, which are bounded by steep scarps and, in many cases, fractured (Figure 6.1). However, there are no obvious tectonic patterns revealed in the global mountain distribution beyond a bimodal variation of number density with longitude (Figure 6.2; Schenk *et al.*, 2001; Kirchoff and McKinnon, 2005) and local associations with paterae, and Io's ubiquitous volcano–tectonic depressions (e.g., Masursky *et al.*, 1979; Whitford-Stark, 1982; Carr *et al.*, 1998; McEwen *et al.*, 2000; Radebaugh *et al.*, 2001; Jaeger *et al.*, 2003; see examples in Figure 6.1). Current evidence indicates that ultimately the mountains do owe their existence to the incredible rate of volcanic resurfacing: the resulting subsidence can induce more than sufficient compressive stresses in the lithosphere, driving mountains up by extensive thrust faulting (Schenk and Bulmer, 1998; Jaeger *et al.*, 2003).

The existence of well over one hundred of these structures imposes constraints on the structure of Io's mechanical lithosphere and their characteristics provide insights into interior and crustal properties. The state of the mountains is intimately related to other geologic processes acting on Io (e.g., both extrusive and intrusive volcanism, Io's internal tidal dynamics, and surficial mass wasting). Therefore, the processes by which the mountains form and evolve have implications for many different aspects of Io. In this chapter we describe the current state of understanding, derived from *Voyager* and *Galileo* observations and analyses thereof, of Io's mountains, their formation and evolution, and the implications for Io's tectonics and lithosphere.

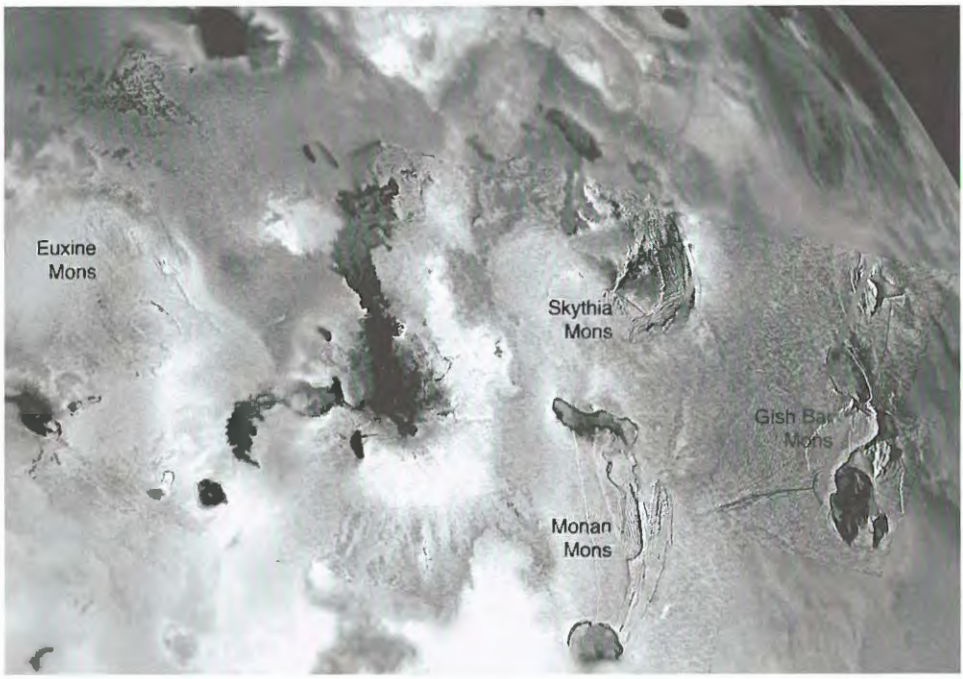

Figure 6.1. This moderate-resolution, ~500 m per pixel, regional mosaic combined with lower resolution, 1.3 km per pixel, color images acquired by *Galileo* includes several examples of Ionian mountains and volcanic centers. The mountains are isolated from each other, but a high fraction of those in this region are associated with paterae. The illumination, which is from the left, accentuates the topography and surface textures. This effect is strongest on the eastern side where the solar incidence angle is 21–28° and weakens toward the west where the Sun is higher, solar incidence angle ~37–45°: compare the visibility of ~10 km high Gish Bar Mons, between Gish Bar Patera to the south and Estan Patera to the north; ~6 km high Monan Mons, between Monan Patera to the north and Ah Peku Patera to the south; and ~7 km high Euxine Mons. (See also color section.)

6.2 OBSERVATIONS

6.2.1 Global distribution

Here we use the term "mountain" generally to refer to landforms that rise significantly (>~1 km) above the surrounding terrain, regardless of their specific morphologic classification (mesas, plateaus, peaks, ridges, etc.). As a whole these structures are typically on the order of 100 km across and rise to heights of several kilometers above the surrounding plains (e.g., Schaber, 1980; Carr *et al.*, 1998), with a mean height of ~6 km and a maximum (to date) of 17.5 ± 1.5 km, at Boösaule Montes (Schenk *et al.*, 2001). Carr *et al.* (1998) documented ~100 Ionian mountains and plateaus in images from the *Voyager* and early *Galileo* missions. Since then Schenk *et al.* (2001) and

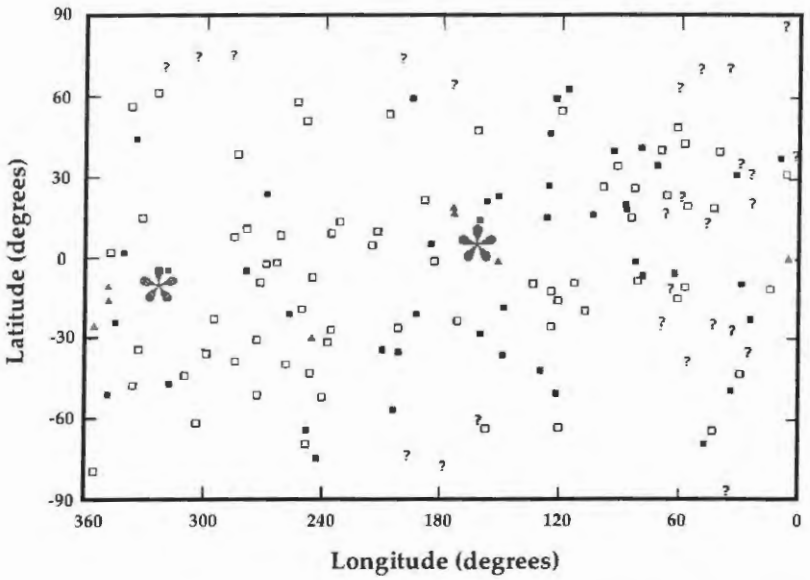

Figure 6.2. A plot of the locations of Ionian mountains (small symbols) reported by Carr *et al.* (1998), Schenk *et al.* (2001), and Jaeger *et al.* (2003; also Jaeger, 2005), as verified by Jaeger (2005) and updated here to include the locations of prominent shield volcanoes identified in Schenk *et al.* (2004) (cf. Appendix 2). The symbol ▲ is used for volcanic constructs, ■ for tectonic mountains in contact with at least one patera, □ for tectonic mountains that do not contact any paterae, and ? for mountains whose relationship to paterae could not be determined. The two regions identified by Schenk *et al.* (2001) as having higher concentrations of volcanic centers (and lower concentrations of mountains) are indicated by large asterisks.

Jaeger *et al.* (2003; also Jaeger, 2005) have further refined databases of the characteristics of Io's topographic structures, bringing the total number of mountains reported to 151; however, not all of the features identified in the early study were confirmed by the later investigations. The number of positively identified Ionian mountains is converging on ~135, with some uncertainty remaining for features with borderline heights (~1 km) and/or ambiguous morphologies (Appendix 2), or for which the viewing conditions were unfavorable. (NB. One significant complicating factor is that the ability to detect even several-km-high mountains in images depends strongly upon the solar incidence angle. Io's surface is highly variegated and regions are frequently blanketed by material erupted from plumes, so although mountainous regions can have distinctive textures and sometimes colors, even the most rugged terrains are not necessarily apparent as such when viewed at high Sun angles (i.e., in the absence of topographic shading).)

The mountains are typically isolated from each other. There are no patterns in their distribution that suggest organized global-scale tectonic processes such as terrestrial plate tectonics. Carr *et al.* (1998) noted no obvious correlations between Io's mountains and its numerous hot spots and plumes; however, they did note an

apparent association between mountains and paterae that had also been observed by Masursky *et al.* (1979). More recent studies based on the complete *Galileo* data set have demonstrated that the global distribution of mountains exhibits two moderate enhancements in number density centered around 25°N, 65°W and 20°S, 265°W (Figure 6.2; e.g., Schenk *et al.*, 2001; Kirchoff *et al.*, 2003; Kirchoff and McKinnon, 2005). Intriguingly these regions are essentially anticorrelated with two peaks identified in the distributions of features identified as (or in some cases inferred based on albedo and/or color to be) volcanic centers of all types, at longitudes of 165°W and 325°W (Schenk *et al.*, 2001) and of paterae at longitudes of 150°W and 330°W (Radebaugh *et al.*, 2001).

The apparent global anticorrelation between mountains and volcanic features makes all the more curious the observations that at the local scale a significant fraction of mountains seems to be closely associated with paterae (e.g., Masursky *et al.*, 1979; Schaber, 1980; Whitford-Stark, 1982; McEwen *et al.*, 2000). Indeed, McEwen *et al.* (2000) examined images taken by the *Galileo* spacecraft during its first three close Io fly-bys, finding that, of the 13 mountains imaged at resolutions higher than 0.5 km per pixel, 6 are incised by paterae. These mountains are located within a region of relatively high mountain density and low volcanic center density (Schenk *et al.*, 2001; Kirchoff and McKinnon, 2005). Including all of the *Galileo* observations, Jaeger (2005) showed that, of the 97 mountains identified as tectonic, 40 (41%) are in *direct* contact with paterae, calculating the probability of this correlation occurring by chance to be less than ~1%. Based on the refined mountain statistics presented here (Appendix 2), of 104 mountains likely to be tectonic in origin, 39 (38%) contact paterae. For comparison, of the 417 paterae imaged at pixel scales less than 3.2 km that were documented by Radebaugh *et al.* (2001), only 13% are in contact with mountains. More recent harmonic analysis by Kirchoff *et al.* (2003; see also Kirchoff and McKinnon, 2005), confirms these results: for small order and degree (comparable with global-scale wavelengths) there is an anti-correlation of mountains and volcanic centers, but at higher order and degree correlations are observed.

6.2.2 Morphology

Io's mountains (again, using the term to encompass elevated landforms in general) exhibit significant morphologic variety (e.g., Figures 6.1 and 6.3–6.6). Only a few seem to be volcanic constructs (e.g., Carr *et al.*, 1998; McEwen *et al.*, 2000; Schenk *et al.*, 2001; Jaeger *et al.*, 2003): mountains rarely appear to have vents or calderas at, or flows emanating from, their summits and none correspond to identified hot spots or vent regions for active plumes. Instead, most appear to have tectonic origins, resembling uplifted or tilted blocks (e.g., Carr *et al.*, 1998, Schenk and Bulmer, 1998), and often exhibiting steep scarps and fractures (e.g., McEwen, 1985; McEwen *et al.*, 2000; Turtle *et al.*, 2001, 2004; Jaeger *et al.*, 2003). Of the 135 mountains documented in Appendix 2, six appear to be volcanoes. The rest appear likely to be tectonic in origin but have considerable morphologic diversity, which complicates interpretation. For example, Io has numerous low-lying (several hundred meters to ~1 kilometer) mesa-like topographic features with irregular margins. Several such features are included in

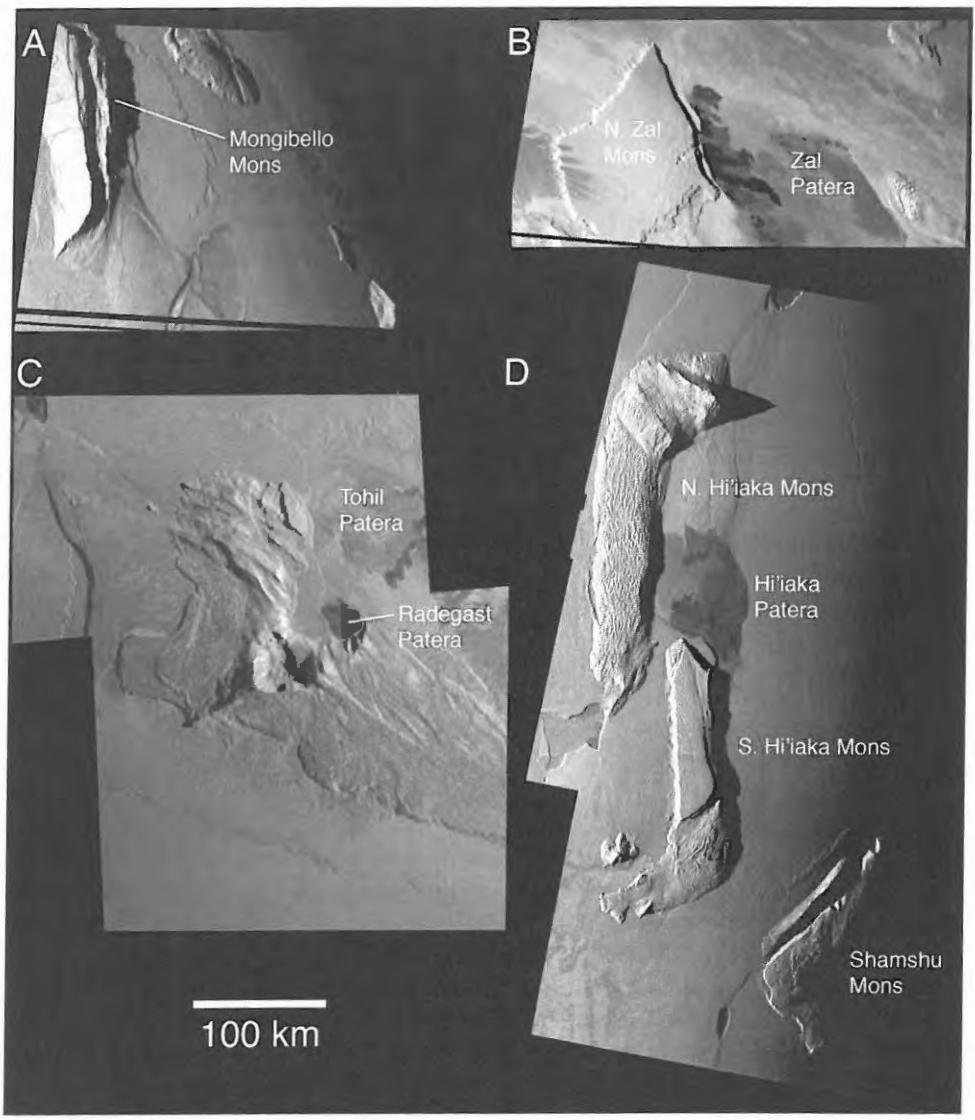

Figure 6.3. *Galileo* images of Ionian mountains: (A) Near-terminator view of Mongibello Mons (jagged double ridge at left) at 335 m per pixel, illuminated from the left. (B) Near-terminator view of North Zal Montes and Zal Patera at ~260 m per pixel, illuminated from the left. To the north-west the mountain is smooth with arcuate margins, whereas its south-eastern margin is slumping outward in long landslides. Lava flows emanate from a fracture that parallels the eastern margin of North Zal Montes. (C) Moderate-resolution, ~325 m per pixel, mosaic of Tohil Mons and neighboring Tohil and Radegast Paterae seen near the terminator, illumination is from the right (cf. Figure 6.4). (D) Near-terminator view of Hi'iaka and Shamshu Montes at ~360 m per pixel, illuminated from the left.

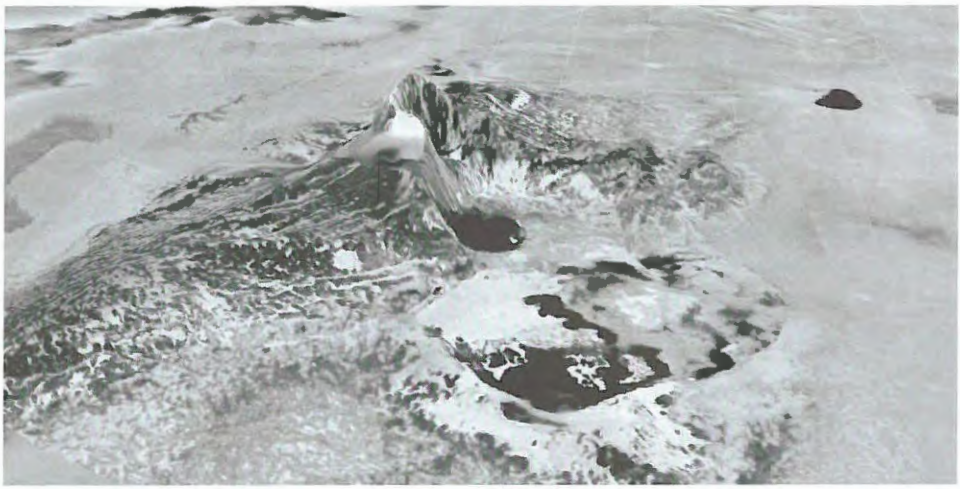

Figure 6.4. Perspective view of Tohil Mons looking south-west. Color-coding represents topography (red is high) (see color section). Topography is derived from stereo analysis by P. Schenk. Tohil Mons is comprised of several parts, including a broad lineated plateau to the east (left in this view) truncated by a small dark patera (center), and a circular, faulted plateau to the north-west (right). Each plateau is 3–5 km high, and between them lies a circular amphitheater with a crest rising 8 km above the surrounding plains. Vertical exaggeration is a factor of ~25.

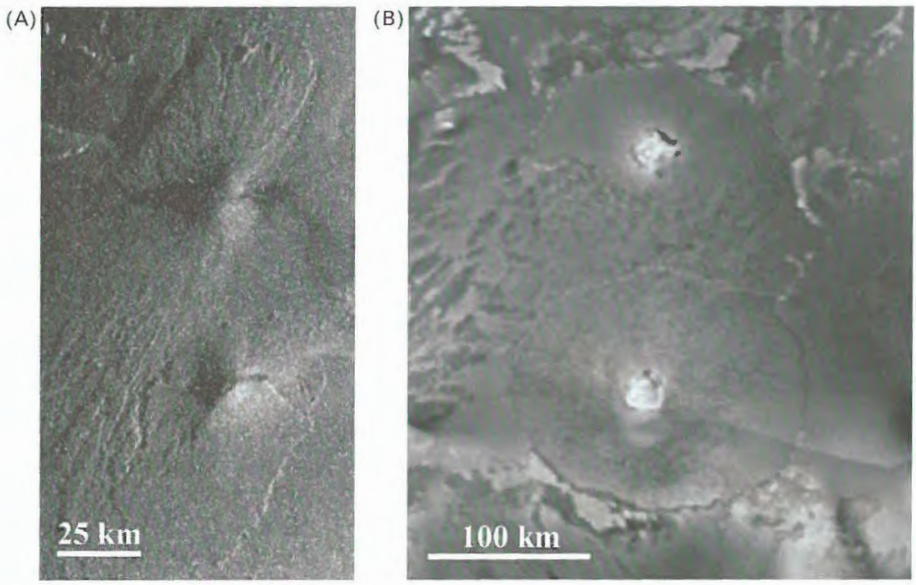

Figure 6.5. Examples of mountains classified as volcanic structures. (A) Two shield volcanoes located near the plume Zamama at 16.8°N, 173.7°W and 18.7°N, 174.4°W. (B) Apis Tholus (10.9°S, 348.7°W) and Inachus Tholus (15.8°S, 348.8°W), which are substantially larger than other Ionian volcanic constructs.

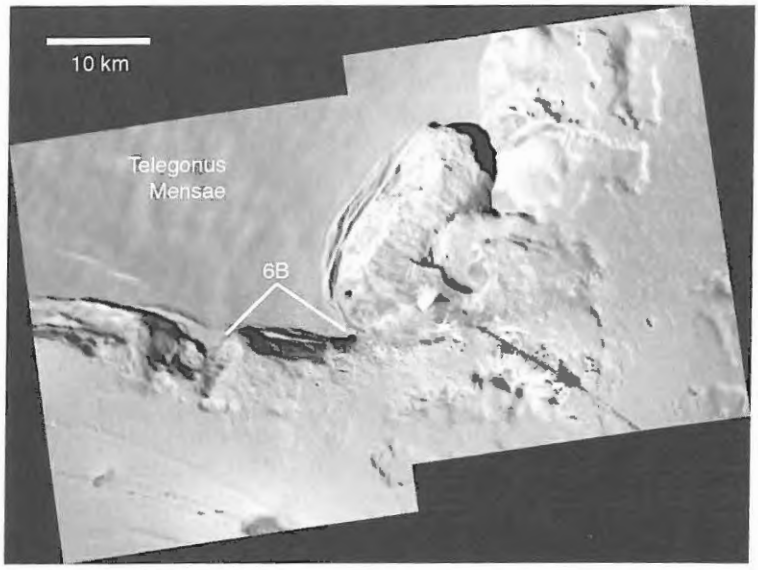

(A)

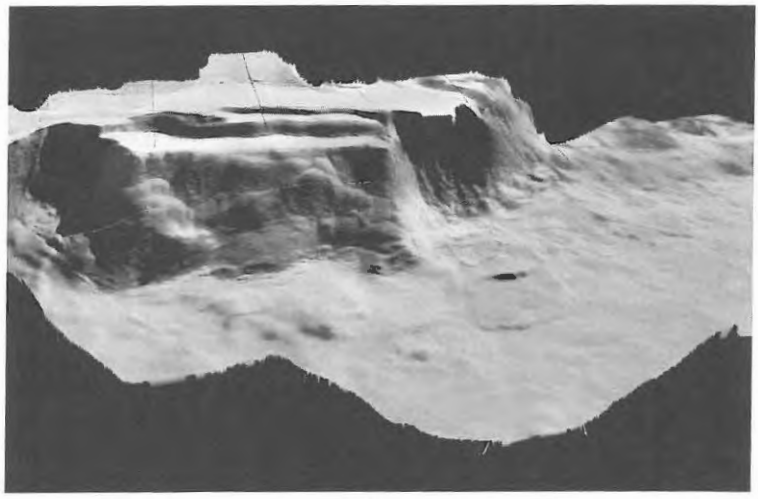

(B)

Figure 6.6. (A) High-resolution (42 m per pixel) mosaic of the south-eastern margin of Telegonus Mensae. The label 6B indicates the section of the scarp illustrated in (B). Illumination is from the upper right. (B) Perspective view of southern scarp of Telegonus Mensae looking north. Color-coding represents topography (red is high) (see color section); total relief is ~1.5 km. Topography is derived from stereo analysis by P. Schenk. A small (~4 km long, ~2 km wide), low (~100 m) landslide is evident at center right. Note the wrinkled appearance of the scarp and terrace face, suggesting down-slope creep of surface material. Vertical exaggeration is a factor of ~50.

Appendix 2 because their heights slightly exceed 1 km, but their origins remain uncertain; possibilities include eroded lava plains and degraded tectonic structures. Therefore, the number of tectonic mountains in Appendix 2 is conservatively estimated to be 104 by excluding all mountains that exhibit volcanic morphologies, those that were not imaged well enough to determine their gross morphology, and all structures not conclusively determined to be $\geq$2 km in height (to filter out the genetically ambiguous low-lying mesas). Their morphologies range from jagged peaks (e.g., Figures 6.3(C,D) and 6.4) and ridges (e.g., Figure 6.3(A)) several kilometers high, to lower, more rounded structures with gentler slopes (e.g., Monan Mons in Figure 6.1, see also color section), to low, flat-topped or tilted plateaus with steep margins (e.g., Figures 6.3(B) and 6.6). The margins of many structures show evidence of outward collapse through slumping and large landslides (e.g., Skythia and Gish Bar Montes in Figure 6.1) and a few have steeper, scalloped scarps (e.g., Figure 6.3(B); see also further examples of mountain morphologies in Schenk and Bulmer, 1998; Moore *et al.*, 2001; McEwen *et al.*, 2000; Turtle *et al.*, 2001, 2004). In some cases, morphologic differences, which are sometimes observed across a single structure, may simply illustrate variations in the deterioration of mountains by mass wasting or heterogeneities in the composition, volatile content, and material properties of the Ionian crust. For example, tall, rugged mountains might be more likely to form in silicate-rich regions and lower plateaus in regions with more sulfur-rich compounds. Moreover, these variations could be influenced by different mountain formation mechanisms and local lithospheric conditions, such as the thermal gradient.

Structural control

Several morphologic characteristics of Ionian mountains support the hypothesis that they are tectonic in origin. Many of the structures have strikingly straight, angular, or curvilinear margins (e.g., Hi'iaka Mons and the ridge and valley to the west of Shamshu Mons (Figure 6.3(D)) and North Zal Mons (Figure 6.3(B))). Other mountains have linear elements, or assemblages within them, for example the scarps that cut the center of Skythia Mons (Figure 6.1, see also color section), the ridges that make up Mongibello (Figure 6.3(A)) and Ionian Montes, and the ridge running south-west from the peak of Tohil Mons (Figures 6.3(C) and 6.4). However, in most cases, the orientations of the structural features of neighboring mountains do not appear to be related to each other. Another aspect of several mountains that is consistent with tectonic origins is their asymmetric profiles: for example, Euboea Mons (Schenk and Bulmer, 1998) and Gish Bar Mons (Turtle *et al.*, 2001) have relatively steep scarps on one side with gentler slopes on the other, suggestive of tilted crustal blocks. In fact, in each of these cases it appears that the surface layers along the shallower slopes have failed in massive landslides (Schenk and Bulmer, 1998; Turtle *et al.*, 2001).

The *Galileo* images also revealed a few examples of what appear to be linear surface fractures: a scarp that is several hundred kilometers long and up to 1.5 kilometers high runs south along the eastern edge of North Zal Mons (Figure 6.3(B)) and, intriguingly from a tectonic standpoint, the *western* edge of South Zal

Mons; smaller fractures are observed in the plains to the east of Telegonus Mensae and along the eastern margin of Skythia Mons; and a Y-shaped feature cuts the plains to the west of Gish Bar Patera (Figure 6.1; a higher resolution view is available in Turtle *et al.*, 2004, Figure 10a). The first two of these exhibit evidence for recent volcanic activity (Turtle *et al.*, 2001, 2004). However, there is little information about the topography of these features aside from the upper limit on the height of the one east of North Zal Mons (Turtle *et al.*, 2001), so whether they are strictly sites of extension or of incipient mountain building cannot be assessed. To be visible despite Io's high rate of resurfacing, these features would have to be relatively young; at the present estimated resurfacing rate, 0.1–1 cm yr^{-1} averaged globally (e.g., Johnson *et al.*, 1979; Blaney *et al.*, 1995; Phillips, 2000; McEwen *et al.*, 2004), it would only take 10^4–10^5 years to bury 100 m of topography, and the rate of degradation by mass wasting may be even higher.

Relationship to volcanism

Although rare, there are a few topographic structures that do appear to have volcanic origins (Figure 6.5). The most significant of these are the Tholi, Apis, and Inachus (Figure 6.5(B)), that were observed by *Voyager* (sadly a spacecraft anomaly during *Galileo*'s only close fly-by of the sub-Jovian hemisphere resulted in the loss of its only opportunity to observe these intriguing features (Turtle *et al.*, 2004)). These circular structures are ~1.5 km high with central caldera-like depressions 2–3 km deep (Schenk *et al.*, 2004). Most of Io's radial volcanic flow fields appear to be relatively low, broad shield volcanoes, including the two 2-km-high shield volcanoes just west of the Zamama flow field (Figure 6.5(A); Schenk *et al.*, 2004; Turtle *et al.*, 2004) and very shallow Emakong Patera (Williams *et al.*, 2001). *Galileo* observations of the site of the Zamama plume and flow field (Turtle *et al.*, 2004) revealed that the lava flows emanate from one of two conical volcanic constructs (as predicted by Keszthelyi *et al.*, 2001) that are up to 2 km high (based on shadow measurements and photoclinometry). Nearby Tsũi Goab Tholus (Turtle *et al.*, 2004, Figure 11; Williams *et al.*, 2004), appears to be a smaller shield volcano with two depressions near its summit, and another similar cone is located near Pele (Moore *et al.*, 1986); however, in general, such structures are rare on Io.

Some paterae appear to be incised into low plateaus or broad, shield-like features (e.g., Chaac, Thomagata, and Reshef Paterae). For example, 56 km by 26 km Thomagata Patera is 1.2–1.6 km deep (based on measurements of the shadows cast by the patera walls) and set into a raised plateau more than 100 km across, the western margin of which rises only ~200 m above the plain (Turtle *et al.*, 2004). It is not clear whether these structures were created by eruptions from the paterae, or if they were pre-existing topographic features that have been eaten away by the formation of the paterae.

Although few of the mountains are actual volcanic constructs, as previously mentioned, there is a statistically significant correlation between mountains and paterae: the margins of 41% of well documented mountains are in direct contact with at least one patera, 12% are in contact with two or more paterae (Jaeger *et al.*,

2003; Jaeger, 2005). One region with a concentration of such relationships is the area encompassing Euxine Mons and Gish Bar Mons (Figure 6.1). Euxine Mons itself, almost completely surrounds a circular depression, which may be a patera that has not erupted recently. Monan Mons directly abuts two paterae: to its north lies the oddly shaped Monan Patera, which Lopes-Gautier *et al.* (1999) identified as an active hot spot, and which exhibits deposits of the red material that is commonly associated with active volcanic venting (McEwen *et al.*, 1998a; Geissler *et al.*, 1999; Lopes-Gautier *et al.*, 1999; Phillips, 2000) at its margins; and to the south lies another patera, Ah Peku. Gish Bar Patera appears to eat into an apparent landslide deposit from Gish Bar Mons to the north, which is in turn, bordered to the north by a second patera, Estan Patera. Indeed the only large mountain in this region that is not associated with a patera is Skythia Mons, although it too is bordered by a fracture that may also exhibit some small reddish deposits, which would be consistent with current or very recent volcanic activity. The associations of mountains with paterae are more common than one would expect from unrelated, spatially random distributions of mountains and paterae; Jaeger (2005) derived that the probability of the observed correlation occurring by chance is less than ~1%.

Surface modification and mass wasting

The modification and degradation of Ionian mountains also provide key insights into the types of surficial processes active on Io and their rates (e.g., Moore *et al.*, 2001), and the *Galileo* images have revealed a few places on the surface in great detail, ~10 m per pixel. Though the mountains are thought to expose the oldest rock units on Io (e.g., Smith *et al.*, 1979; Schaber, 1980), no impact craters have been identified on them. Therefore, their crater retention ages must be younger than 10^6–10^7 years (Johnson *et al.*, 1979; Zahnle *et al.*, 2003; McEwen *et al.*, 2004), which is not terribly surprising given that modification of their surfaces appears to be dominated by mass-wasting processes and deposition of material from volcanic plumes. To some extent the variations in mountain morphology may illustrate an aging sequence for Ionian mountains, from steep, angular peaks (e.g., Gish Bar and Hi'iaka Montes (Figures 6.1 and 6.3(D)), to gentler, more rounded slopes (e.g., Monan and western Shamshu Montes (Figures 6.1 and 6.3(D)). However, significant variations in morphology within individual structures or complexes (e.g., Tvashtar (Turtle *et al.*, 2001; Turtle *et al.*, 2002, Figure 7) and Telegonus (Figure 6.6)), indicate that the differences cannot be due solely to age; there must also be heterogeneities in the compositional, rheological, structural, and thermal properties of the crust at scales of 10s–100s of kilometers.

Slumping and landsliding dominate at both large and small scales (e.g., Figure 6.6) and can occur in close proximity to each other, demonstrating spatial variation in material properties, including porosity and the presence of liquid filling the pore spaces, over distances of several kilometers. Many topographic structures have hummocky surface textures which appear to be due to massive outward slumping (e.g., the southern margin of the eastern patera of Tvashtar Catena (Turtle *et al.*, 2002, their fig. 7) and the eastern and south-western margins of Skythia Mons (Figure 6.1)).

In a number of places, the headscarps of discrete landslides can be seen (e.g., Skythia Mons, N. Zal Montes, and Telegonus Mensae (Figures 6.1, 6.3(B), and 6.6(A), respectively). Although suspected to be a site of possible sapping due to its morphology as seen at lower resolution and an association of very bright material, presumably SO_2, Telegonus was revealed by *Galileo* images to be the site of gravity driven mass wasting in the form of slumps, downslope creep, and landslides (Figure 6.6(B)). Amphitheaters on the south-eastern margin and straight scarps along the ~1.5 km high (from measurements of stereo observations, Figure 6.6(B)) southern margin exhibit morphologies typical of slumping: flat-topped blocks with hummocky textures along their bases. Interestingly, there are slope-parallel lobes (up to ~1 km long) on the face of this block that suggest some manner of downslope creep; the average slope of the scarp can be constrained by the illumination geometry to be less than 26°. Near the scarp's eastern edge a succession of at least three landslides can be seen, the most extensive of which is 3.8 km long, 2.1 km wide, and less than 100 m thick at its distal end (Figure 6.6(B)).

Some mountains are covered with ridges that parallel the mountains' margins (e.g., Monan Mons and northern Hi'iaka Montes (Figures 6.1 and 6.3(D)). Superficially similar features are observed in regions without obvious topography (Bart *et al.*, 2004), but where slopes are clear the ridges may be caused by folding of a thin, detached surface layer sliding downslope under the influence of gravity (Heath, 1985; Moore *et al.*, 2001). By approximating this as a single elastic layer under compression Turtle *et al.* (2001) estimated its thickness to be $\sim 70\,\text{m} \leq h \leq \sim 550\,\text{m}$ from the wavelength of the folds and approximations for other surface parameters. The amplitudes and wavelengths of ridges on individual mountains appear to be generally uniform even though there are some differences in ridge morphology from mountain to mountain. If the ridges are caused by slip along a weak stratigraphic boundary, the uniformity would suggest that there is little variation in the slope of the detachment surface and that the mountains were uplifted and tilted as fairly coherent blocks despite the pervasively fractured nature of the Ionian lithosphere. In the case of North Hi'iaka Mons, stereo data presented by Schenk *et al.* (2001) show a gently and relatively uniformly sloped plateau.

6.2.3 Stratigraphy

Surprisingly there is little direct evidence for layering within Io's crust, although circumstantial evidence abounds. The simple fact that the crust forms by continual burial of materials ranging from silicate lava flows to volatile plume deposits, requires that it consist of interbedded materials of varying properties, and, as discussed previously, extensive layers of sulfur-rich material, presumably pyroclastic in origin, may provide the zones of weakness implied by massive slope failures as Schenk and Bulmer (1998) suggested occurred at Euboea Montes. There are also hints of layers observed in some high-resolution observations (e.g., Tohil and Ot Montes (the latter is shown in Turtle *et al.*, 2002, Figure 2)). However, there is no unambiguous evidence for layering in the very-high-resolution (9.6 m per pixel) views of the southern scarp of Telegonus Mensae (Turtle *et al.*, 2004, Figure 5b). Layers a

few tens of meters thick would be resolved directly and thinner, ledge-forming layers should also be evident; however, mass-wasting processes appear to dominate the scarp's morphology, masking any small-scale, internal structure. In a few places (e.g., Shamshu and Tohil Montes), very bright areas are visible on scarps, which may indicate that SO_2 is being exposed by erosion or seeping out of the scarps in these locations.

There is some morphologic evidence (e.g., surrounding Tvashtar Catena (Turtle *et al.*, 2002, their fig. 7) and near Telegonus Mensae (Figure 6.6(A))) for erosion by sapping as McCauley *et al.* (1979) hypothesized would result from liquefied SO_2 seeping out at the bases of steep scarps, although sublimation degradation or disaggregation by chemical decomposition may be more realistic thermodynamically if sapping is occurring away from geothermal anomalies (Moore *et al.*, 2001). Below these arcuate scarps the terrain often consists of a series of thin, layered deposits and occasional kilometer-scale blocks and hummocks, which may be landslide debris or remnants of coherent, volatile-poor material left behind when the less consolidated material was eroded. Given that Io's plateaus commonly stand at least several hundred meters above the surrounding plains, the relative paucity of such material (at least inasmuch as can be constrained at the image resolutions currently available) would indicate that the SO_2 is able to carry away fine-grained sulfur and silicate particles quite efficiently as it vaporizes and expands into the Ionian atmosphere (Moore *et al.*, 2001).

6.3 INTERPRETATIONS AND IMPLICATIONS

6.3.1 Mountain formation mechanism(s)

An elegant solution to the apparent irony of the mountains on such an incredibly volcanically active planet not being volcanoes themselves was proposed by Schenk and Bulmer (1998). Io's global average volcanic resurfacing rate over the past few decades is estimated to be $\sim 1\,\mathrm{cm\,yr^{-1}}$ (Johnson *et al.*, 1979; Blaney *et al.*, 1995; Phillips, 2000; McEwen *et al.*, 2004) if due primarily to lava flows, although uncompressed plume deposits could yield much higher resurfacing rates (Phillips, 2000). Furthermore, over the short time period of the *Voyager–Galileo* era, the resurfacing rate has been observed to vary widely over the surface of the planet (Phillips, 2000; Geissler *et al.*, 2004), although it may tend to average out globally over geologic timescales (e.g., Carr *et al.*, 1998). At a rate of $1\,\mathrm{cm\,yr^{-1}}$ it would only take 10^6 years for the current surface to become buried to a depth of 10 km. So the rapid resurfacing rate drives comparably rapid subsidence.

Considering the crust as a series of spherical, progressively older shells, as each shell is buried deeper and deeper its radius, and consequently its surface area, decreases, generating horizontal compressive stresses throughout the lithosphere. Within several kilometers of the surface, these stresses exceed the compressive strength of rock and they are a likely driving mechanism for uplifting Io's mountains by thrust faulting. Moreover, the magnitude and continual generation

of these stresses suggests that Io's lithosphere should be pervasively fractured. This manner of mountain building is consistent with the correlation observed between mountains and paterae on the local scale: depending on the local geology, in some cases orogenic thrust faults may serve to alleviate compressive crustal stresses sufficiently that the faults can act as conduits along which magma can ascend to the surface (Turtle *et al.*, 2001; Jaeger *et al.*, 2003). Another consequence of the rapid subsidence rate is that lithospheric temperatures remain quite cold to great depths (O'Reilly and Davies, 1981), only undergoing significant heating within a narrow zone near the base of the lithosphere; therefore, assuming efficient remixing of heated crustal material with the mantle, the crust and the mechanical lithosphere would be essentially identical.

A hypothesis for the observed global-scale anticorrelation of mountains and volcanic centers is that a sustained reduction in Io's volcanic activity on a local, regional, or global scale would allow more extensive conductive lithospheric heating, and that the resulting thermal expansion would induce compressive stresses at the base of the lithosphere (McKinnon *et al.*, 2001). In this scenario, fluctuations in the thermally induced stresses due to variations in resurfacing rates could lead to alternating episodes of compressive and tensile faulting in the upper part of the lithosphere. McKinnon *et al.* (2001) hypothesized that, as a consequence of repeated normal and reverse faulting, Io's surface might be analogous to the chaos terrain of Europa with coherent crustal blocks (i.e., mountains) floating within a matrix of highly disrupted material. This scenario would be consistent with other interpretations of some mountains having undergone extensional faulting as McEwen (1985) and Heath (1985) suggested for Danube Planum, although other proposed mountain formation mechanisms do not preclude post-orogenic extensional stresses.

Jaeger *et al.* (2003) compared the stresses from mechanical and thermal sources (i.e., subsidence and conductive heating, respectively) and found that, ignoring the localized effects of intrusions and assuming a uniform resurfacing rate of 1 cm yr^{-1}, the peak stress generated by thermal expansion can exceed that caused by subsidence for lithospheres thinner than about 40 km. However, the integrated effect of thermal expansion on lithospheric compression is not as great as that of subsidence: the subsidence induced stress is large for much of the lithosphere (Figure 6.7), while, for current estimates of the resurfacing rate (Johnson *et al.*, 1979; Carr, 1986; Blaney *et al.*, 1995; Phillips, 2000; McEwen *et al.*, 2004; Geissler *et al.*, 2004), only the lowermost lithosphere is significantly heated (O'Reilly and Davies, 1981). Thus, while the stresses induced by thermal expansion can locally exceed those produced by subsidence, they act on a much smaller fraction of the lithosphere.

The stresses of global subsidence and thermal expansion are sufficient to generate significant uplift on Io by compressional faulting. However, these stresses alone cannot explain the isolated nature of the distribution of Ionian mountains. Schenk and Bulmer (1998) suggested that failure could be triggered by crustal anisotropies or localized weakening or fracturing due to volcanic activity. Turtle *et al.* (2001) demonstrated using numerical simulations that, without such focusing mechanisms, global compressive stresses acting on an extensively faulted, uniform lithosphere would be likely to produce parallel mountain ranges rather than isolated massifs. Therefore,

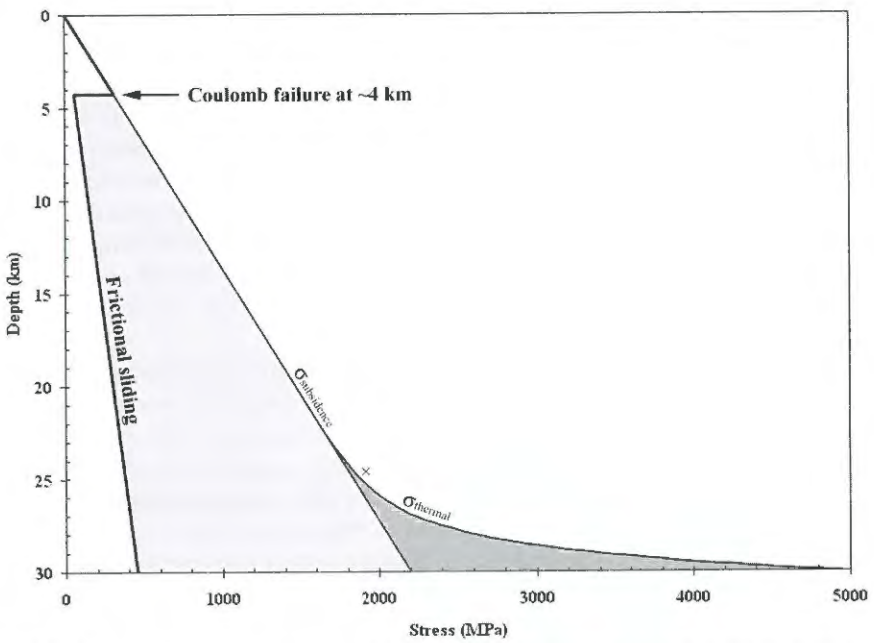

Figure 6.7. The compressive strength of the Ionian lithosphere and the magnitude of the compressive horizontal stress ($\sigma_{\text{subsidence}} + \sigma_{\text{thermal}}$) as a function of depth for a 30-km-thick lithosphere. The maximum compressive strength of Io's lithosphere at the surface is assumed to be 275 MPa (the maximum compressive strength of unconfined rock samples of gabbro and several other rock types (Ahrens, 1995)). Thrust faults are assumed to form at 30°, and the resurfacing rate is assumed to be 1 cm yr^{-1}. The resulting equation for Coulomb failure is $\tau = 79.4 + 0.58\sigma_n$, where τ is the critical shear stress (in MPa) and σ_n is the normal stress (in MPa). On Io, the compressive horizontal stress due to subsidence is sufficient to initiate faulting at a depth of ~4 km. Once faults exist, stress should be relieved by slip along these pre-existing planes of weakness. According to Byerlee's Law, frictional sliding is governed by the equation $\tau_f = 0.85\sigma_n$, where τ_f is the shear stress at which sliding begins. The solid black line illustrates the approximate stress state of the lithosphere and the shaded regions show the stress in excess of this that is available to drive mountain uplift. The ligbt gray region shows the magnitude of the compressive stress due to subsidence and the dark gray region shows the contribution of thermal expansion.

there must be a mechanism or mechanisms that localize the lithospheric compressive stresses. Jaeger *et al.* (2003) investigated the role that the dynamics of Io's asthenosphere may play in focusing stresses. Models for Io's interior suggest an asthenospheric layer at least 50–200 km thick, which is strongly heated by tidal dissipation (e.g., Segatz *et al.*, 1988; Spohn, 1997; Keszthelyi *et al.*, 1999; Ross *et al.*, 1990; Radebaugh, 2005; Ojakangas and Stevenson, 1986; Greenberg, 1982; Schubert *et al.*, 2004). Modeling by Tackley *et al.* (2001) suggests that the interior of Io is likely to be vigorously convecting, an idea that is well supported by the large number of hot spots scattered about Io's surface. Wherever thermally buoyant asthenospheric

diapirs impinge on the base of the lithosphere, the overlying material is thinned and upwarped (e.g., Crough, 1979, 1983; Sleep, 1992), an idea applied to Io by McEwen (1995). Such lithospheric swells should focus horizontal compressive stresses into an inverted conic shape expanding from the base of the lithosphere over the diapir head and intersecting the surface at the perimeter of the swell (see Jaeger *et al.*, 2003, Figure 10). This stress pattern is corroborated by axially symmetric, 2-D, finite-element modeling that takes into account the surface curvature of Io (Turtle *et al.*, 2001). In the most simplistic case, failure along a sector of this cone will result in a thrust fault with an arcuate trace, a common feature of thrust faults and one that is observed at several mountains on Io (e.g., Monan Mons (Figure 6.1)). However, the length scale and characteristic spacing of mountains may not necessarily correspond to the diameter of a swell; a single swell could influence the formation of multiple mountains. Additionally, more complex stress patterns would arise where heterogeneities exist or wherever there is interference between stress fields induced by neighboring lithospheric swells. Multiple thrust-fault localization mechanisms are almost certainly at work: spatial variations in material properties and lithospheric structure, as well as spatial and temporal variations in the resurfacing rate and thermal conditions, will result in localizing stresses in the lithosphere, thereby facilitating the uplift of mountains as isolated structures rather than as ordered thrust belts.

The diapiric focusing mechanism would also be consistent with the observed correlation between mountain and patera formation: once the stress has been alleviated by mountain uplift, magma supplied by the thermal diapir could buoyantly rise toward the surface using the overlying fractures and faults as conduits for its ascent. Because the thrust fault is a compressive interface, magma may ascend more readily at tear faults along the margins of the thrust sheet. If thrust faulting over-shortens material in the upper lithosphere as McKinnon *et al.* (2001) suggest, extension may also occur at the trailing edge of a thrust sheet. Once thrust faulting effectively dissipates the local compressive stress, magma may use the thrust fault plane as a conduit as well.

Monan Mons displays a number of the features predicted by such a model. The diapir focusing mechanism predicts a circular concentration of compressive stress at the surface, which is likely to produce a thrust fault with an arcuate trace, although this fault profile alone is not diagnostic of the diapir model. Crescent shapes are common in thrust faults because they allow for maximum compression at the center of the thrust sheet and progressively less slip toward the margins. At Monan Mons the trace of the thrust fault is concave westward, which would indicate that the hanging wall moved east (Elliot, 1976; see also Jaeger, 2005, Figure 2.11). Faults or fracture zones that are not subject to a large compressive stress make more likely conduits for magma ascent. The trailing edge of a thrust sheet is one such region, and the shear zones that bound a thrust sheet are others. Therefore, paterae may preferentially form at these locations. Monan Patera is an elongate depression with active volcanism occurring around its margin as indicated by red deposits (cf., McEwen *et al.*, 1998a; Geissler *et al.*, 1999; Lopes-Gautier *et al.*, 1999; Phillips, 2000). Its longitudinal axis is roughly perpendicular to that of the adjacent mountain, consistent with what would be expected if Monan Patera were situated along a sinistral shear zone at the edge of a

thrust sheet (Figure 6.1; Jaeger, 2005, Figure 2.11). Moreover, there is also a patera at the dextral shear zone on the opposite side of the thrust sheet (i.e., at the opposite end of the mountain).

The morphology of the Hi'iaka Montes (~7.4°S, ~78.7°W; Figure 6.3(D)) suggests an intriguing hypothesis regarding their tectonic evolution. Both mountains consist of ~4 km high, north–south ridges that slope gently downward to the west (Schenk *et al.*, 2001), the shapes of which are strikingly complementary: the northern end of North Hi'iaka Mons consists of a ~11 km high peak where the mountain extends to the east, and the southern end of South Hi'iaka Mons appears to consist of a landslide deposit where it hooks to the west. The geometry of these mountains suggests that they may once have formed a single massif that subsequently sheared apart along a dextral (right-lateral) strike–slip fault (McEwen *et al.*, 2000). The planimetric shapes of the north and south margins of Hi'iaka Patera and the volcano–tectonic depression separating the two mountains, lend credence to this hypothesis. Apart from a landslide headscarp in the north, the two margins' planimetric shapes are identical over the entire ~50 km of their lengths. If the northern patera margin were translated ~70 km to the south it would match up with its southern counterpart. These observations hint at unique regional-scale shear deformation within the Hi'iaka Montes complex, although they are not conclusive (a further *Galileo* observation planned to observe Hi'iaka under different illumination conditions to help constrain this history was lost due to a spacecraft anomaly (Turtle *et al.*, 2004)).

6.3.2 Lithospheric thickness

Io's lithosphere has generally been assumed to need to be tens of kilometers thick in order to form and support mountains of the observed heights (e.g., Nash *et al.*, 1986; Carr *et al.*, 1998). The thrust faulting scenario for mountain building outlined above provides another constraint on the thickness of the lithosphere. As resurfacing buries a shell of material from Io's surface to the base of the lithosphere, its effective radius is reduced and it is heated. Jaeger *et al.* (2003) calculated the lithospheric volume change due to subsidence and thermal expansion as a function of lithospheric thickness by integrating the strain in a shell of material over depth. Conservation of volume dictates that any reduction in volume at depth be balanced by an uplift of the same volume at the surface. By comparing the total estimated volume of Io's mountains with the estimated lithospheric volume loss, Jaeger *et al.* (2003) placed a lower limit of 12 km on Io's lithospheric thickness (Figure 6.8), consistent with estimates based on intact mountain heights (Schenk *et al.*, 2001). This value is a lower limit because (1) additional material can be accommodated by means other than mountain uplift (e.g., compaction of pore space or broad, low uplifts) and (2) the base levels from which mountain heights were measured could have been too high (e.g., mass wasting deposits around mountains could have artificially elevated the levels from which the heights were measured). These calculations can also place a weak upper limit on lithospheric thickness. For example, if the lithosphere of Io were 50 km thick, as was used in one model by Keszthelyi and McEwen (1997), nearly

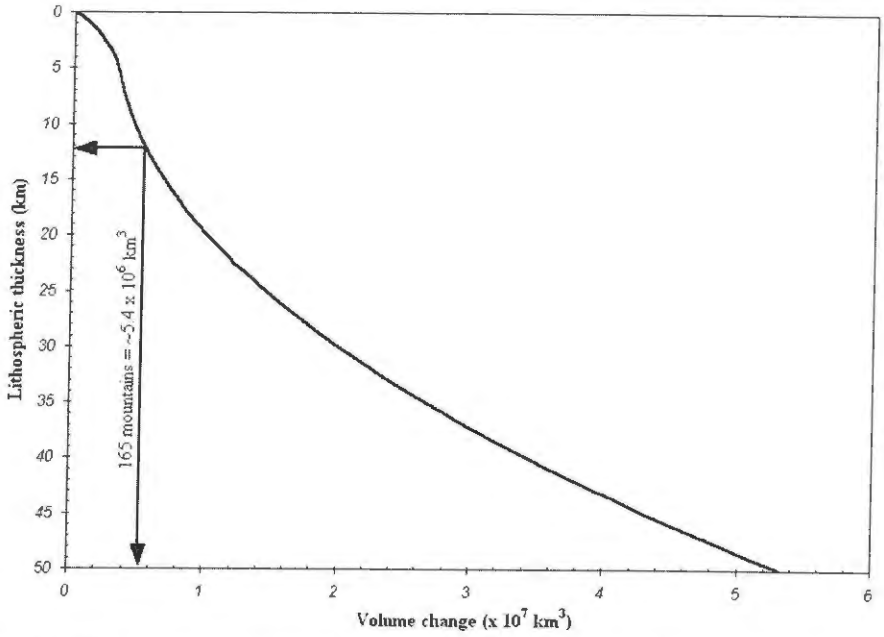

Figure 6.8. The estimated volume of uplifted material is the sum of the volumes of material displaced by subsidence stresses, thermal expansion, and the extent to which the compressibility of lithospheric rock can counteract those processes, plotted as a function of lithospheric thickness (after Jaeger, 2005, Figure 2.8). The upper limit of 165 Ionian mountains (extrapolated from the upper limit of the number of mountains observed, 145, to account for the lack of global coverage) would correspond to ~54 million km^3 of material which yields a lower limit of ~12 km for the lithospheric thickness; the observed number of 145 mountains corresponds to roughly 47 million km^3 and a slightly lower value for the lower limit on lithospheric thickness.

48 million km^3 of material, the equivalent of >1,450 average-sized mountains (Schenk *et al.*, 2001), would need to be accommodated in ways other than mountain uplift. Leone and Wilson (2001) estimated that Io's uppermost crust could have a porosity as high as ~30%; compaction of such pore space could accommodate a significant volume of material. Much volume could also be concealed in broad, regional uplifts with shallow, and therefore difficult to detect, topography. Gaskell *et al.* (1988) reported such basins and swells using *Voyager* data, but these were not matched by analyses of the *Galileo* data (Thomas *et al.*, 1998; Oberst and Schuster, 2004), which are not subject to the geometric distortions of *Voyager* imaging. So in each case any long-wavelength topography may represent residual error. Regional variations in elevation appear to be limited to no more that ±1 km from the mean triaxial ellipsoid (Thomas *et al.*, 1998; Oberst and Schuster, 2004). Given these uncertainties a lithospheric thickness of 50 km might be reasonable; however, extremely thick lithospheres (e.g., ≥100 km (Ross and Schubert, 1985; Anderson *et al.*, 2001)), become difficult to reconcile due to the excessive amount of uplifted material that would need to have gone undetected.

6.3.3 Crustal composition and stability

The great heights of the mountains suggest that the crust consists of a strong silicate component, although the low thermal gradient (O'Reilly and Davies, 1981) does to some extent mitigate the concern of Clow and Carr (1980) that a crust composed predominantly of sulfur-rich materials would be able to support only the lowest topographic features observed (~1 km). Nonetheless, based on the extent of silicate volcanism that has been observed (e.g., McEwen *et al.*, 1998b; Keszthelyi *et al.*, 2001; McEwen *et al.*, 2004; and references therein), Io's crust is expected to have a significant silicate component.

There is ample evidence for the existence of weaker, more volatile materials within the crust. For example, vast landslides appear to have occurred at Euhoea and Gish Bar Mons (Schenk and Bulmer, 1998; McEwen *et al.*, 2000). There are also widespread eroding layered plains (e.g., Schaber, 1980) as well as several examples of higher scarps that appear to be retreating, but which have left surprisingly little debris. In cases where mountains abut paterae, there are only a few examples where debris from small landslides from the mountains can be seen on the floors of the paterae (e.g., Gish Bar, Shamshu, Radegast, and Hi'iaka Paterae). This observation indicates that volcanic resurfacing is proceeding more rapidly than the mass wasting of the mountains. It furthermore suggests that a large proportion of the material that collapses from mountains into paterae, which are hypothesized to be manifestations of lava lakes (Lopes *et al.*, 2004), is consumed, an idea which is easier to explain if a substantial fraction of the material is volatile. However, in some cases, especially those of catastrophic landslides, the massive deposits could make such drastic alterations to patera boundaries that we might not be able to identify them as such.

Volcanic resurfacing on Io adds new material to the top of the crust at a rapid rate and the fate of this material as it is buried deeper and deeper within the crust, and of that material that eventually reaches the base of the crust, is of fundamental importance to understanding Io. Assuming that the crust is not growing thicker, it must be recycled back into the mantle at a comparable rate. It is possible that this transition is entirely thermal: a shell of crustal material subsides and heats up, eventually to the point that the timescale for it to become entrained in convection is shorter than that of subsidence. Another possibility is that blocks of material at the base of the crust are plucked by drag forces induced by the convecting asthenosphere. A third possibility is that, as the intense compression associated with subsidence drives out volatiles and collapses pore spaces, the lower crust becomes denser than the underlying material and delaminates along pre-existing zones of structural weakness. Jaeger *et al.* (2004) examined this last possibility by starting with a variety of bulk silicate compositions for Io, evolving the crust and mantle iteratively via volcanic reprocessing until equilibrium was achieved, and then modeling the density structure of the crust. The evolution of Io's crust and mantle from the bulk silicate starting composition was determined using the MELTS program (Ghiorso and Sack, 1995; Asimow and Ghiorso, 1998) for a range of upper mantle temperatures. Jaeger *et al.* (2004) made several assumptions in modeling the crust's density profile: (1) they used the geothermal gradient of O'Reilly and Davies (1981); (2) they assumed a subsidence rate

of 1 cm yr^{-1} (and the analysis is quite sensitive to this parameter); (3) because subsidence generates large compressive stresses at a rapid rate, they assumed that the stress state is governed by Byerlee's/Amonton's law of frictional sliding; (4) their crust (as derived from bulk silicate) was generally of a mafic igneous composition, and they assumed that SO_2 fills the pore space in this rock but does not get interbedded with it to any significant depth; and (5) they assumed a porosity of 25% at the surface and an exponential decrease with depth (Leone and Wilson, 2001). They found that the crust of Io would be gravitationally unstable if upper mantle temperatures exceed ~1,600 K: density inversions between the lower crust and upper mantle were found to exist over a narrow range of upper mantle temperatures (~1,550–1,600 K). This density inversion is conducive to crustal recycling by delamination. These findings initially seemed at odds with observational constraints on internal temperatures (e.g., a lower limit on magma liquidus temperature of ≥1,870 K was derived from data from a 1997 eruption at Pillan (Davies *et al.*, 2001). As more is learned about Ionian magma temperatures and the complexities of the derivation thereof, the highest temperature estimates have been revised down somewhat such that the two approaches are now in good agreement (Radebaugh *et al.*, 2004; Milazzo *et al.*, 2005); however, such constraints are generally restricted to lower limits on liquidus temperatures.

6.4 CONCLUSIONS

A better understanding of the processes responsible for forming Io's mountains is emerging from the data from both the *Voyager* and *Galileo* missions, and continued analysis thereof. Io's rapid resurfacing results in a unique tectonic environment in which the tremendous compressional stresses, induced by the high subsidence rate, fracture the cold lithosphere and uplift mountains by thrust faulting. The lack of a global tectonic pattern can be explained by heterogeneities in the lithospheric composition, structure, and stress field, which serve to focus the stresses with random orientations, thereby localizing mountain building. Many if not all such lithospheric heterogeneities can also be attributed to variations in volcanic activity. For example, spatial and temporal changes in the style of volcanic activity (e.g. changes in the proportion of volatiles deposited), will significantly affect the strength of the lithosphere. A change in the rate of volcanic activity will be reflected in the subsidence rate and therefore the thermal profile of the lithosphere in that region, perhaps explaining the bimodal variation observed in the number of mountains with longitude. Activity within the asthenosphere, such as local upwellings, will affect the stress field in the overlying lithosphere, preferentially facilitating faulting in some regions. And, of course, thrust faulting itself will alleviate local compressional lithospheric stresses, thereby making it easier for magma to rise along the same faults and perhaps even reach the surface to form paterae at the mountains' feet (cf., Keszthelyi *et al.*, 2004). At first glance, it appears surprising that Io's mountains are not volcanoes; nonetheless, despite their tectonic nature, their origins are ultimately a consequence of Io's extreme level of volcanic activity.

6.5 REFERENCES

Ahrens, T. J. 1995. *Rock Physics and Phase Relations: A Handbook of Physical Constants*. American Geophysical Union, Washington D.C.

Anderson, J. D., R. A. Jacobson, E. L. Lau, W. B. Moore, and G. Schubert. 2001. Io's gravity field and interior structure. *J. Geophys. Res.*, **106**, 32963–32969.

Asimow, P. D. and M. S. Ghiorso. 1998. Algorithmic modifications extending MELTS to calculate subsolidus phase relations. *American Mineralogist.*, **83**, 1127–1132.

Bart, G. D., E. P. Turtle, W. L. Jaeger, L. P. Keszthelyi, and R. Greenberg. 2004. Ridges and tidal stress on Io. *Icarus*, **169**, 111–126.

Blaney, D. L., T. V. Johnson, D. L. Matson, and G. J. Veeder. 1995. Volcanic eruptions on Io: Heat flow, resurfacing, and lava composition. *Icarus*, **113**, 220–225.

Carr, M. H. 1986. Silicate volcanism on Io. *J. Geophys. Res.*, **91**, 3521–3532.

Carr, M. H., A. S. McEwen, K. A. Howard, F. C. Chuang, P. Thomas, P. Schuster, J. Oberst, G. Neukum, G. Schubert, and the Galileo Imaging Team. 1998. Mountains and calderas on Io: Possible implications for lithospheric structure and magma generation. *Icarus*, **135**, 146–165.

Clow, G. D. and M. H. Carr. 1980. Stability of sulfur slopes on Io. *Icarus*, **44**, 729–733.

Crough, S. T. 1979. Hotspot epeirogeny. *Tectonophysics*, **61**, 321–333.

Crough, S. T. 1983. Hotspot swells. *Ann. Rev. of Earth and Planet. Sci.*, **11**, 165–193.

Davies, A. G., L. P. Keszthelyi, D. A. Williams, C. B. Phillips, A. S. McEwen, R. M. C. Lopes, W. D. Smythe, L. W. Kamp, L. A. Soderblom, and R. W. Carlson. 2001. Thermal signature, eruption style, and eruption evolution at Pele and Pillan on Io. *J. Geophys. Res.*, **106**, 33079–33104.

Elliot, D. 1976. The energy balance and deformation mechanism of thrust sheets. *Phil. Trans. R. Soc. Lond. A.*, **283**, 289–312.

Gaskell, R. W., S. P. Synnott, A. S. McEwen, and G. G. Schaber. 1988. Large-scale topography of Io: Implications for internal structure and heat transfer. *Geophys. Res. Lett.*, **15**, 581–584.

Geissler, P. E., A. S. McEwen, L. Keszthelyi, R. Lopes-Gautier, J. Granahan, and D. P. Simonelli. 1999. Global color variations on Io. *Icarus*, **140**, 265–282.

Geissler, P., A. S. McEwen, C. B. Phillips, L. P. Keszthelyi, and J. Spencer. 2004. Surface changes on Io during the Galileo mission. *Icarus*, **169**, 29–64.

Ghiorso, M. S. and R. O. Sack. 1995. Chemical mass transfer in magmatic processes. IV: A revised and internally consistent thermodynamic model for the interpolation and extrapolation of liquid–solid equilibria in magmatic systems at elevated temperatures and pressure. *Contrib. Mineral Petrol.*, **119**, 197–212.

Greenberg, R. 1982. Orbital interactions of the Galilean satellites. In: D. Morrison (ed.), *Satellites of Jupiter*. University of Arizona Press, Tucson, AZ, pp. 65–92.

Heath, M. J. 1985. Io: Mountains and crustal extension. *Conference on Heat and Detachment in Crustal Extension on Continents and Planets*. Lunar and Planet. Inst., Houston, TX, Contrib. #575, pp. 50–54.

Jaeger, W. L. 2005. Select problems in planetary structural geology: Global-scale tectonics on Io, regional-scale kinematics on Venus, and local-scale field analysis on Earth application to Mars. Ph.D. thesis, University of Arizona, AZ.

Jaeger, W. L., E. P. Turtle, L. P. Keszthelyi, and A. S. McEwen. 2002. The effect of thrust fault geometries on the surface deformation of Io: Implications for mountains and paterae. *Lunar Planet. Sci. Conf.*, **XXXIII**, Abstract #1741.

Jaeger, W. L., E. P. Turtle, L. P. Keszthelyi, J. Radebaugh, A. S. McEwen, and R. T. Pappalardo. 2003. Orogenic tectonism on Io. *J. Geophys. Res.*, **108**, doi:10.1029/2002JE001946.

Jaeger, W. L., L. P. Keszthelyi, and E. P. Turtle. 2004. Lithospheric recyclying on Io: The role of delamination. *Lunar Planet. Sci. Conf.*, **XXXV**, Abstract #2048.

Johnson, T. V., A. F. Cook II, C. Sagan, and L. A. Soderblom. 1979. Volcanic resurfacing rates and implications for volatiles on Io. *Nature*, **280**, 746–750.

Keszthelyi, L. and A. S. McEwen. 1997. Magmatic differentiation of Io. *Icarus*, **130**, 437–448.

Keszthelyi, L., A. S. McEwen, and G. J. Taylor. 1999. Revisiting the hypothesis of a mushy global magma ocean in Io. *Icarus*, **141**, 415–419.

Keszthelyi, L., A. S. McEwen, C. B. Phillips, M. Milazzo, P. Geissler, D. Williams, E. P. Turtle, J. Radebaugh, D. Simonelli, and the Galileo SSI Team. 2001. Imaging of volcanic activity on Jupiter's moon Io by Galileo during Galileo Europa Mission and Galileo Millennium Mission. *J. Geophys. Res.*, **106**, 33025–33052.

Keszthelyi, L. P., W. L. Jaeger, E. P. Turtle, M. Milazzo, and J. Radebaugh. 2004. A post-Galileo view of Io's interior. *Icarus*, **169**, 271–286.

Kirchoff, M. R. and W. B. McKinnon. 2005. Mountain building on Io: An unsteady relationship between volcanism and tectonism. *Lunar Planet. Sci. Conf.*, **XXXVI**, Abstract #2245.

Kirchoff, M. R., W. B. McKinnon, P. Schenk. 2003. Spherical harmonic analysis of mountain and volcanic center distribution on Io. *EOS Trans. AGU*, **84**, Fall Meet. Suppl., #P41A-0399.

Leone, G. and L. Wilson. 2001. Density structure of Io and the migration of magma through its lithosphere. *J. Geophys. Res.*, **106**, 32983–32995.

Lopes-Gautier, R., A. S. McEwen, W. B. Smythe, P. E. Geissler, L. Kamp, A. G. Davies, J. R. Spencer, L. Keszthelyi, R. Carlson, F. E. Leader, *et al.* 1999. Active volcanism on Io: Global distribution and variations in activity. *Icarus*, **140**, 243–264.

Lopes, R. M. C., L. W. Kamp, W. D. Smythe, P. Mouginis-Mark, J. Kargel, J. Radebaugh, E. P. Turtle, J. Perry, D. Williams, R. W. Carlson *et al.* 2004. Lava lakes on Io? Observations of Io's volcanic activity from Galileo NIMS during the 2001 flybys. *Icarus*, **169**, 140–174.

Masursky, H., G. G. Schaber, L. A. Soderblom, and R. G. Strom. 1979. Preliminary geological mapping of Io. *Nature*, **280**, 725–729.

McCauley, J. F., B. A. Smith, and L. A. Soderblom. 1979. Erosional scarps on Io. *Nature*, **280**, 736–738.

McEwen, A. S. 1985. Hot-spot tectonics on Io. *Conference on Heat and Detachment in Crustal Extension on Continents and Planets*. Lunar and Planet. Inst., Houston, TX, Contrib. #575, pp. 76–80.

McEwen, A. S., SO_2-rich equatorial basins and epeirogeny of Io. *Icarus*, **113**, 415–422.

McEwen, A. S., L. Keszthelyi, P. Geissler, D. P. Simonelli, M. H. Carr, T. V. Johnson, K. P. Klaasen, H. H. Breneman, T. J. Jones, J. M. Kaufman, *et al.* 1998a. Active volcanism on Io as seen by Galileo SSI. *Icarus*, **135**, 181–219.

McEwen, A. S., L. Keszthelyi, J. R. Spencer, G. Schubert, D. L. Matson, R. Lopes-Gautier, K. P. Klaasen, T. V. Johnson, H. W. Head, P. Geissler *et al.* 1998b. High-temperature silicate volcanism on Jupiter's moon Io. *Science*, **281**, 87–90.

McEwen, A. S., M. J. S. Belton, H. H. Breneman, S. A. Fagents, P. Geissler, R. Greeley, J. W. Head, G. Hoppa, W. L. Jaeger, T. V. Johnson *et al.* 2000. Galileo at Io: Results from high-resolution imaging. *Science*, **288**, 1193–1198.

McEwen, A. S., L. Keszthelyi, R. Lopes, P. Schenk, and J. Spencer. 2004. The lithosphere and surface of Io. In: F. Bagenal, W. McKinnon, and T. Dowling (eds), *Jupiter: Planet, Satellites and Magnetosphere*. Cambridge University Press, Cambridge, UK, pp. 307–328.

McKinnon, W. B., P. M. Schenk, and A. Dombard. 2001. Chaos on Io: A model for formation of mountain blocks by crustal heating, melting, and tilting. *Geology*, **29**, 103–106.

Milazzo, M. P., L. P. Keszthelyi, J. Radebaugh, A. G. Davies, E. P. Turtle, P. Geissler, K. P. Klaasen, and A. S. McEwen. 2005. Volcanic activity at Tvashtar Catena, Io. *Icarus*, **179**, 235–251.

Moore, J. M., A. S. McEwen, E. F. Albin, and R. Greeley. 1986. Topographic evidence for shield volcanism on Io. *Icarus*, **67**, 181–183.

Moore, J. M., R. J. Sullivan, F. C. Chuang, J. W. Head, A. S. McEwen, M. P. Milazzo, B. E. Nixon, R. T. Pappalardo, P. M. Schenk, and E. P. Turtle. 2001. Landform degradation and slope processes on Io: The Galileo view. *J. Geophys. Res.*, **106**, 33223–33240.

Nash, D. B., C. F. Yoder, M. H. Carr, J. Gradie, and D. M. Hunten. 1986. Io. In: J. A. Burns and M. S. Matthews (eds), *Satellites*. University of Arizona Press, Tucson, TX, pp. 629–688.

Oberst, J. and P. Schuster. 2004. Vertical control point network and global shape of Io. *J. Geophys. Res.*, **109**, doi:10.1029/2003J002159.

O'Reilly, T. C. and G. F. Davies. 1981. Magma transport of heat on Io: A mechanism allowing a thick lithosphere. *Geophys. Res. Lett.*, **8**, 313–316.

Ojakangas, G. W. and D. J. Stevenson. 1986. Episodic volcanism of tidally heated satellites with application to Io. *Icarus*, **66**, 341–358.

Phillips, C. B. 2000. Voyager and Galileo views of volcanic resurfacing on Io and the search for geologic activity on Europa. Ph.D. thesis, University of Arizona, Tucson, TX, 269pp.

Radebaugh, J. 2005. Formation and evolution of paterae on Jupiter's moon Io. Ph.D. thesis, University of Arizona, Tucson, TX.

Radebaugh, J., L. P. Keszthelyi, A. S. McEwen, E. P. Turtle, W. Jaeger, and M. Milazzo. 2001. Paterae on Io: A new type of volcanic caldera? *J. Geophys. Res.*, **106**, 33005–33020.

Radebaugh, J., A. S. McEwen, M. P. Milazzo, L. P. Keszthelyi, A. G. Davies, E. P. Turtle, and D. D. Dawson. 2003. Observations and temperatures of Io's Pele Patera from Cassini and Galileo spacecraft images. *Icarus*, **169**, 65–79.

Ross, M. N. and G. Schubert. 1985. Tidally forced viscous heating in a partially molten Io. *Icarus*, **64**, 391–400.

Ross, M. N., G. Schubert, T. Spohn, and R. W. Gaskell. 1990. Internal structure of Io and the global distribution of its topography. *Icarus*, **85**, 309–325.

Schaber, G. G. 1980. The surface of Io: Geologic units, morphology, and tectonics. *Icarus*, **43**, 302–333.

Schenk, P. M. and M. H. Bulmer. 1998. Origin of mountains on Io by thrust faulting and large-scale mass movements. *Science*, **279**, 1514–1517.

Schenk, P. M., H. Hargitai, R. Wilson, A. McEwen, and P. Thomas. 2001. The mountains of Io: Global and geological perspectives from Voyager and Galileo. *J. Geophys. Res.*, **106**, 33201–33222.

Schenk, P. M., R. Wilson, and A. Davies. 2004. Shield volcano topography and the rheology of lava flows on Io, 2004. *Icarus*, **169**, 98–110.

Schubert, G., J. D. Anderson, T. Spohn, and W. B. McKinnon. 2004. Interior composition, structure and dynamics of the Galilean satellites. In: F. Bagenal, W. McKinnon, and T. Dowling (eds), *Jupiter: Planet, Satellites and Magnetosphere*. Cambridge University Press, Cambridge, UK, pp. 281–306.

Segatz, M. T., T. Spohn, M. Ross, and G. Schubert. 1988. Tidal dissipation, surface heat flow, and figure of viscoelastic models of Io. *Icarus*, **75**, 187–206.

Sleep, N. H. 1992. Hotspot volcanism and mantle plumes. *Ann. Rev. of Earth and Planet. Sci.*, **20**. 19–43.

Smith, B. A., L. A. Soderblom, T. V. Johnson, A. P. Ingersoll, S. A. Collins, E. M. Shoemaker, G. E. Hunt, H. Masursky, M. H. Carr, M. E. Davies *et al.* 1979. The Jupiter system through the eyes of Voyager 1. *Science*, **204**, 951–972.

Spohn, T. 1997. Tides of Io. In: H. Wilhelm, W. Zurm, and H.-G. Wenzel (eds), *Tidal Phenomena*. Springer, Heidelberg, Germany, pp. 345–377.

Tackley, P. J., G. Schubert, G. A. Glatzmaier, P. Schenk, J. T. Ratcliff, and J.-P. Matas. 2001. Three-dimensional simulations of mantle convection in Io. *Icarus*, **149**, 79–93.

Thomas, P. C., M. E. Davies, T. R. Colvin, J. Oberst, P. Schuster, G. Neukum, M. H. Carr, A. McEwen, G. Schubert, and M. J. S. Belton. 1998. The shape of Io from Galileo limb measurements. *Icarus*, **135**, 175–180.

Turtle, E. P., W. L. Jaeger, L. P. Keszthelyi, A. S. McEwen, M. Milazzo, J. Moore, C. B. Phillips, J. Radebaugh, D. Simonelli, F. Chuang, *et al.* 2001. Mountains on Io: High-resolution Galileo observations, initial interpretations, and formation models. *J. Geophys. Res.*, **106**, 33175–33199.

Turtle E. P., W. L. Jaeger, L. P. Keszthelyi, A. S. McEwen, M. Milazzo, J. Moore, C. B. Phillips, J. Radebaugh, D. Simonelli, F. Chuang, *et al.* 2002. Correction to: Mountains on Io: High-resolution Galileo observations, initial interpretations, and formation models. *J. Geophys. Res.*, **107**, doi:10.1029/2002JE001928.

Turtle E. P., L. P. Keszthelyi, A. S. McEwen, J. Radebaugh, M. Milazzo, D. Simonelli, P. Geissler, D. A. Williams, J. Perry, W. L. Jaeger. 2004. The final Galileo SSI observations of Io: Orbits G28-I33. *Icarus*, **169**, 3–28.

Whitford-Stark, J. L. 1982. The Mountains of Io. *Lunar Planet. Sci. Conf.*, **XIII**, 859–860.

Williams, D. A., R. Greeley, R. M. C. Lopes, and A. G. Davies. 2001b. Evaluation of sulfur flow emplacement on Io from Galileo data and numerical modeling. *J. Geophys. Res.*, **106**, 33161–33174.

Williams, D. A., P. M. Schenk, J. M. Moore, L. P. Keszthelyi, E. P. Turtle, W. L. Jaeger, J. Radebaugh, M. P. Milazzo, R. M. C. Lopes, and R. Greeley. 2004. Mapping of the Culann-Tohil region of Io from Galileo imaging data. *Icarus*, **169**, 80–97.

Zahnle, K., P. Schenk, H. Levison, and L. Dones. 2003. Cratering rates in the outer Solar System. *Icarus*, **163**, 263–389.

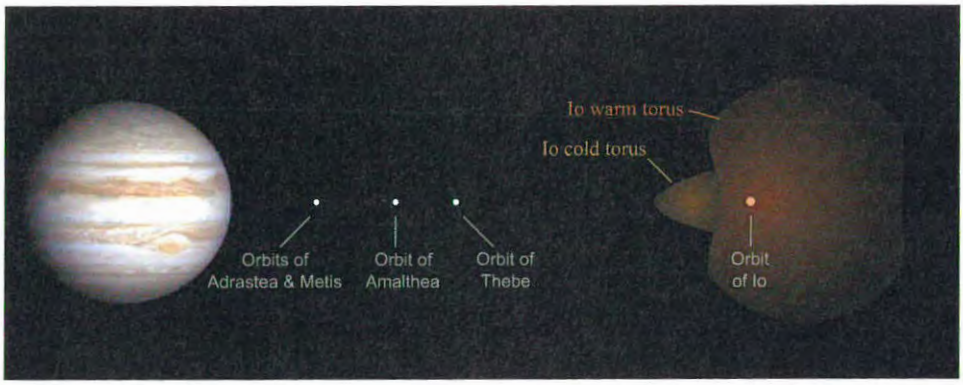

Figure 3.9. This figure illustrates both the warm and cold torus of Io. The *Galileo* spacecraft was able to sample the cold torus on the 34th orbit of Jupiter just before its final trajectory loop around Jupiter on J35. Courtesy Windows to the Universe *www.windows.ucar.edu* A34 Interactive Graphic.

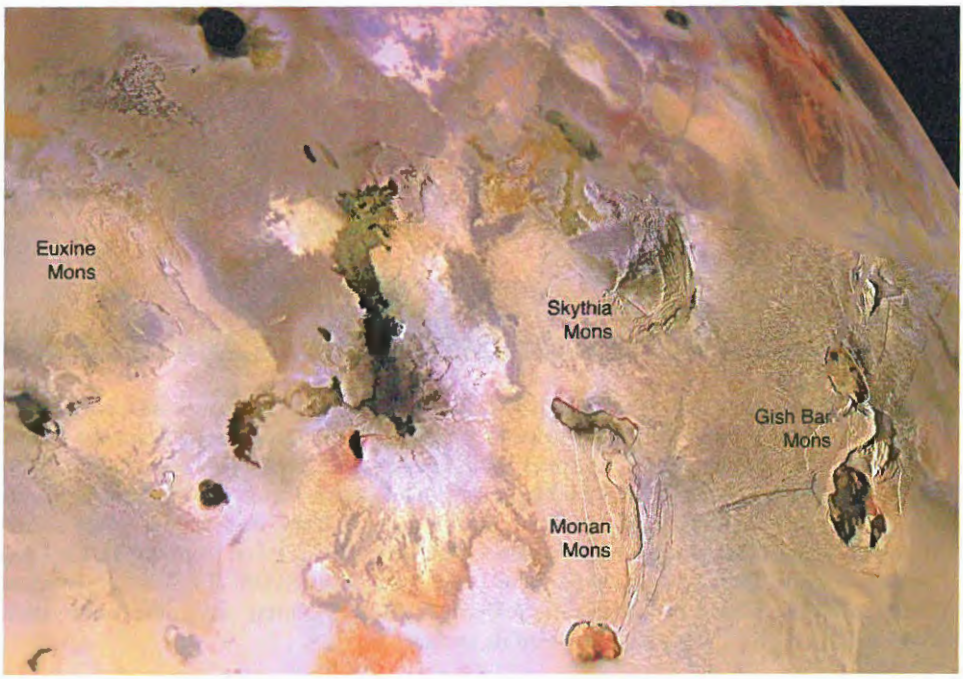

Figure 6.1. This moderate-resolution, ~500 m per pixel, regional mosaic combined with lower resolution, 1.3 km per pixel, color images acquired by *Galileo* includes several examples of Ionian mountains and volcanic centers. The mountains are isolated from each other, but a high fraction of those in this region are associated with paterae. The illumination, which is from the left, accentuates the topography and surface textures. This effect is strongest on the eastern side where the solar incidence angle is 21–28° and weakens toward the west where the Sun is higher, solar incidence angle ~37–45°: compare the visibility of ~10 km high Gish Bar Mons, between Gish Bar Patera to the south and Estan Patera to the north; ~6 km high Monan Mons, between Monan Patera to the north and Ah Peku Patera to the south; and ~7 km high Euxine Mons.

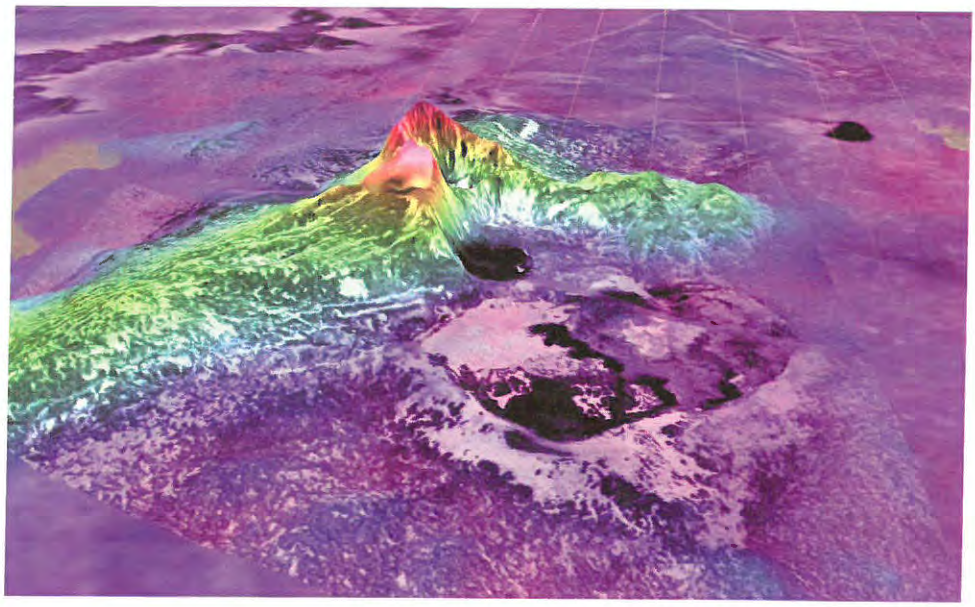

Figure 6.4. Perspective view of Tohil Mons looking south-west. Color-coding represents topography (red is high). Topography is derived from stereo analysis by P. Schenk. Tohil Mons is comprised of several parts, including a broad lineated plateau to the east (left in this view) truncated by a small dark patera (center), and a circular, faulted plateau to the north-west (right). Each plateau is 3–5 km high, and between them lies a circular amphitheater with a crest rising 8 km above the surrounding plains. Vertical exaggeration is a factor of ~25.

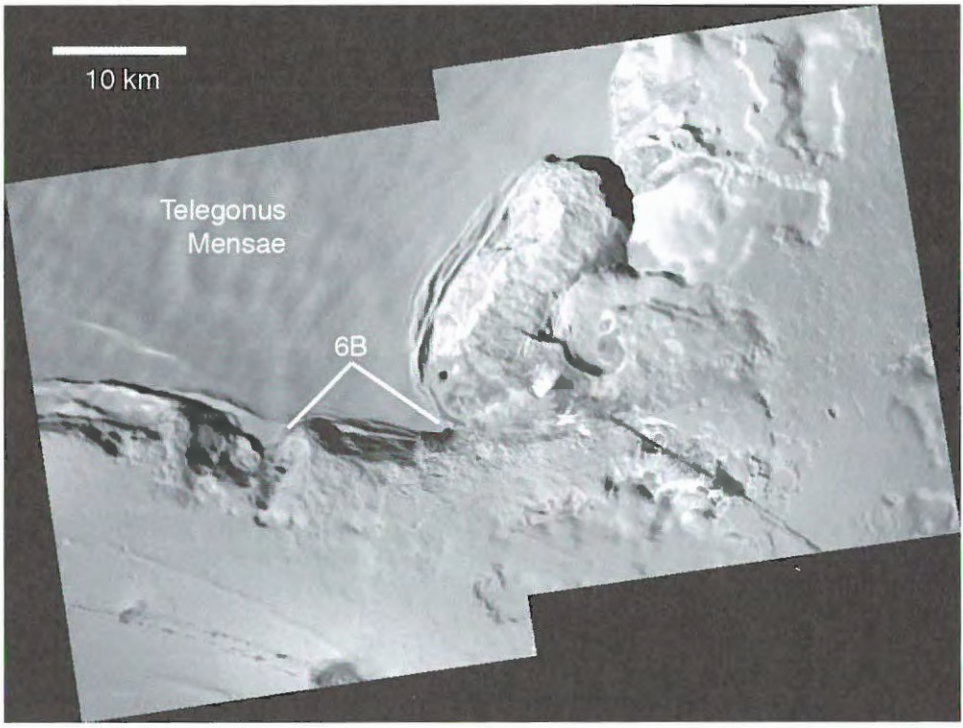

(A)

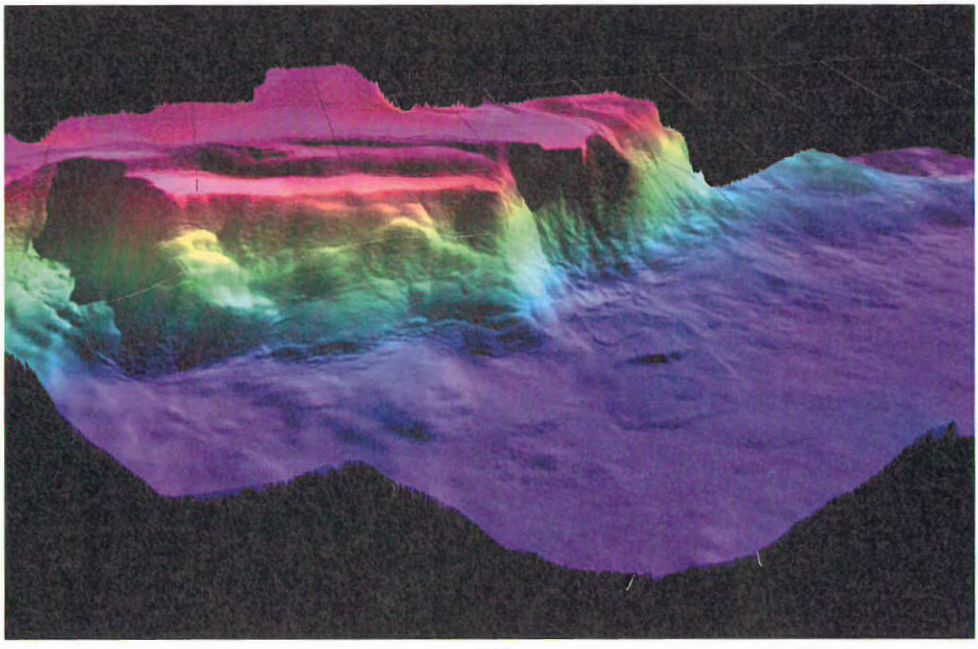

(B)

Figure 6.6. (A) High-resolution (42 m per pixel) mosaic of the south-eastern margin of Telegonus Mensae. The label 6B indicates the section of the scarp illustrated in (B). Illumination is from the upper right. (B) Perspective view of southern scarp of Telegonus Mensae looking north. Color-coding represents topography (red is high); total relief is ~1.5 km. Topography is derived from stereo analysis by P. Schenk. A small (~4 km long, ~2 km wide), low (~100 m) landslide is evident at center right. Note the wrinkled appearance of the scarp and terrace face, suggesting down-slope creep of surface material. Vertical exaggeration is a factor of ~50.